Title

Stereotyped Synaptic Connectivity Is Restored during Circuit Repair in the Adult Mammalian Retina

Journal

Current Biology, 28(11)

ISSN

0960-9822

Authors

Beier, Corinne
Palanker, Daniel
Sher, Alexander

Publication Date

2018-06-01

DOI

10.1016/j.cub.2018.04.063

Peer reviewed

Published in final edited form as:

Curr Biol. 2018 June 04; 28(11): 1818–1824.e2. doi:10.1016/j.cub.2018.04.063.

Stereotyped synaptic connectivity is restored during circuit repair in the adult mammalian retina

Corinne Beier[1,5], **Daniel Palanker**[2,3], and **Alexander Sher**[4,*]

[1.]Electrical Engineering, University of California Santa Cruz, 1156 High Street, Santa Cruz, CA 95064, USA

[2.]Ophthalmology, Stanford University, Stanford, CA 94305, USA

[3.]Hansen Experimental Physics Laboratory, Stanford University, Stanford, CA 94305, USA

[4.]Santa Cruz Institute for Particle Physics, University of California Santa Cruz, 1156 High Street, Santa Cruz, CA 95064, USA

[5.]Present address: Section on Light and Circadian Rhythms, National Institute of Mental Health, 35 Convent Drive, Bethesda, MD 20892, USA

SUMMARY

Proper function of the central nervous system (CNS) depends on the specificity of synaptic connections between cells of various types. Cellular and molecular mechanisms responsible for the establishment and refinement of these connections during development are the subject of an active area of research [1–6]. However, it is unknown if the adult mammalian CNS can form new type-selective synapses following neural injury or disease. Here, we assess whether selective synaptic connections can be reestablished after circuit disruption in the adult mammalian retina. The stereotyped circuitry at the first synapse in the retina, and the relatively short distances new neurites must travel compared to other areas of the CNS, make the retina well suited to probing for synaptic specificity during circuit reassembly. Selective connections between short-wavelength sensitive cone photoreceptors (S-cones) and S-cone bipolar cells provides the foundation of the primordial blue-yellow vision, common to all mammals [7–18]. We take advantage of the ground squirrel retina, which has a one-to-one S-cone to S-cone bipolar cell connection, to test if this connectivity can be reestablished following local photoreceptor loss [8,19]. We find that after *in-vivo* selective photoreceptor ablation, deafferented S-cone bipolar cells expand their dendritic trees. The new dendrites randomly explore the proper synaptic layer, bypass M-cones, and selectively synapse with S-cones. However, non-connected dendrites are not pruned back to

[*]Lead Contact. Correspondence should be addressed to sashake3@ucsc.edu.

AUTHOR CONTRIBUTIONS

C.B. designed and performed experiments, analyzed and interpreted data, and wrote the manuscript. D.P. designed experiments and wrote the manuscript. A.S. designed experiments, interpreted data, and wrote the manuscript.

DECLARATION OF INTEREST

The authors declare no competing interests.

resemble unperturbed S-cone bipolar cells. We show, for the first time, that circuit repair in the adult mammalian retina can recreate stereotypic selective wiring.

eTOC Blurb

Beier *et al.* show that after the ablation of S-cone photoreceptors, S-cone bipolar cells in the adult ground squirrel retina restructure their dendrites to make new synapses with the surviving S-cone photoreceptors. This demonstrates that adult mammalian CNS neurons can reestablish stereotyped synaptic connectivity after injury or disease.

RESULTS

Deafferented S-cone bipolar cells increase their dendritic field

We used immunohistochemistry to identify S-cones and S-cone bipolar cells in the ground squirrel retina after selectively ablating a small patch of photoreceptors with a laser (ablation zones were 0.1–0.2mm wide by 1mm long). In the ground squirrel retina, S-cone bipolar cells can be identified with an antibody against HCN4 (Figure 1A) [19]. S-cone axon terminals are distinguishable from M-cone axon terminals by the lack of ionotropic glutamate receptor 5 (iGluR5) channels at their ribbon synapses (Figure 1B) [7]. An antibody against S-opsin, which brightly stained the outer segments and, more dimly, the cell bodies of S-cones, was used to verify the location of S-cones (Figure 1A, B).

S-cone bipolar cells in the ground squirrel retina are normally post-synaptic to a single S-cone [8,19]. S-cone bipolar cell dendritic trees typically consist of a single stalk (Figure 1A, D). Occasionally in healthy retina, dendritic branches will form from the base of the dendritic stalk and either return to the primary stalk or, more rarely, contact another S-cone [19].

Since the S-cone bipolar cell dendritic field is small (consisting of a single cone), local photoreceptor ablation by *in vivo* selective laser photocoagulation completely deafferents these cells (Figure 1C, D). The destruction of photoreceptors results in the disappearance of pre-synaptic photoreceptor ribbons and the post-synaptic markers, iGluR5 and metabotropic glutamate receptor 6 (mGluR6) (Figure 1E, F) [20]. One week after the ablation, the dendritic stalks of the deafferented S-cone bipolar cells appear to be undisturbed (Figure 1D) and their dendritic tips remain in the outer plexiform layer (OPL) (Figure 1C). Some evidence of early restructuring may be visible in the fine structure of the dendritic tips of the deafferented bipolar cells (Figure 1C insets), which are known to respond within hours after photoreceptor loss in mouse retina [21].

With time, S-cone bipolar cells significantly restructure their dendritic trees in response to deafferentation. Dendritic branches and elongated dendrites are readily visible 60 days after photoreceptor ablation (Figure 2A, B). The new dendritic branches travel parallel to the OPL and thereby increase the dendritic field area (Figure 2C). The deafferented S-cone bipolar cells continue to expand their dendritic trees with lesion age, at least until the end of the 150-day follow-up period (correlation coefficient = 0.85, $p < 2e\text{-}4$, Figure 2C).

To test if the new dendritic branches exhibited a direction preference towards available photoreceptors outside the ablation zone, we measured the vector sum of each cell's dendritic projections. We did not observe an obvious dendritic direction preference from the cells inside the ablation zone (Figure 2D). To quantify this measurement, we calculated the directionality index (DI) of each cell (see Methods). S-cone bipolar cells did not show a clear direction preference in their dendrites, even in older ablation zones (Figure 2E).

Deafferented S-cone bipolar cells make new synapses with S-cones

To determine if deafferented S-cone bipolar cells make new synapses with S-cones outside the ablation zone, we looked at the deafferented S-cone bipolar cells whose dendrites cross the ablation zone edge into the photoreceptor-rich areas (n = 145 edge cells from 10 lesions 30-days and older). Even though only 6% of the ground squirrel cones are S-cones [22], we find that the dendritic branches of 51% (n = 74/145) of the edge cells terminate at an S-cone axon terminal. An example of such a contact is shown in Figure 3A. The S-cones approached by edge cells are significantly more likely to be approached by more than one S-cone bipolar cell when compared to the rest of the S-cones (Figure 3B, binomial test, p = 0.048 for 30 day, p = 1e-7 for 60 day, p = 2e-7 for 110 day, and p = 5e-13 for 135–150 day old ablation zones ages). This increased divergence of S-cone to S-cone bipolar cells confirms that the approaching dendrites are new. It also indicates that the restructured dendrites are not displacing the dendrites of the original post-synaptic S-cone bipolar cell.

To test if the fraction (51%) of the edge cells with dendrites terminating at an S-cone axon terminal can be achieved randomly, we rotated the cone mosaic 180 degrees around the lesion center. The traced bipolar cell dendrites were not changed in any way. This transformation preserves the statistics of the cone mosaic and the overlap between the cones and the dendrites of the edge cells. Only 20% (n = 31/145) of the edge cells had dendrites that terminated at an S-cone axon terminal after the cone mosaic transformation. This fraction is significantly smaller than the 51% (n = 74/145) of successful edge cells we actually observed (binomial probability, p = 1e-12). This shows that dendritic terminations of the deafferented S-cone bipolar cells at S-cone axon terminals cannot be explained by random chance. The follow-up question then is: if the dendritic terminations at S-cones are not random, do the encounters with S-cone axon terminals occur randomly? Interestingly, we find that 52% (n= 76/145) of S-cone bipolar cell dendrites encountered the S-cone axon terminal (either terminated at or continued beyond) in the mirrored cone mosaic. This is the same fraction we saw in successful termination of the edge cells at S-cone axon terminals (binomial probability, p = 0.66). These observations indicate that deafferented S-cone bipolar cells first encounter S-cones by random search, but then selectively terminate their dendrites at the S-cone axon terminal.

To determine if the restructured S-cone bipolar cell dendrites terminating at S-cone axon terminals form new synapses with the S-cones, we compared the amount of mGluR6 at the new contacts to that at unaffected synapses. We hypothesized that the overlap volume between the HCN4-labeled S-cone bipolar cell dendrites and mGluR6 antibody stain at the S-cone synapses (see Methods, Figure 3C) would differ between S-cones that diverged to 2 instead of 1 S-cone bipolar cell. Indeed, in the healthy retina, the volume of mGluR6 and

HCN4 overlap at S-cone axon terminals providing input to two bipolar cells was significantly larger than for the S-cones connected to a single S-cone bipolar cell (Student's t test, p = 8e-5, Figure 3D). We found that the mGluR6/HCN4 overlap for the S-cone axon terminals approached by edge cells was also significantly larger than that for the non-divergent S-cones (p = 0.0011), and consistent with the overlap for the divergent S-cones (p = 0.92) in the healthy retina. This result suggests that restructured dendrites of the deafferented S-cone bipolar cells form new synapses with S-cones and that the S-cone bipolar cells originally connected to these S-cones retain their synapses.

S-cone bipolar cell dendrites that find new S-cones travel within M-cone territory before finding their new synaptic partners. We find that dendrites will reach, on average, 10μm into M-cone territory and bypass 2 M-cone axon terminals (cone axon terminal diameter ~5μm), with some dendrites traveling much greater distances (> 20μm) before contacting an S-cone (Figure 3E). Furthermore, we rarely (17%, n = 4/23 edge cells) see an overlap between a restructured S-cone bipolar cell dendrite and the mGluR6 stain under an M-cone axon terminal (Figure 3C). Together, these observations indicate that the restructured dendrites are making preferential synaptic contacts with S-cones while bypassing the more populous M-cones.

Deafferented S-cone bipolar cells that find S-cones do not simplify their dendritic trees

Pruning the unsuccessful dendrites is a strategy used frequently during neural development. If the same approach is used for the observed selective rewiring of the S-cone bipolar cells, we would expect the successful edge cells to prune their unsuccessful dendritic branches so that the new dendritic structure resembles the healthy S-cone bipolar cell with a single stalk reaching to a single S-cone. We find that deafferented S-cone bipolar cells that have found a new S-cone do not prune their additional dendritic branches (Figure 4A, binomial probability comparing unsuccessful deafferented edge cells with edge cells that find S-cones, p > 0.06). Furthermore, the dendritic field areas of the successful and unsuccessful S-cone bipolar edge cells are indistinguishable from one another (Figure 4B, KS test, p > 0.8). S-cone bipolar cells that find new S-cones in the adult retina do not simplify their dendritic tree back to a single stalk.

DISCUSSION

Proper function of the central nervous system depends on the specificity of synaptic connections between cell types. Complete circuit reassembly in the adult CNS will require both proper targeting of distant brain regions as well as precision at the synaptic scale. Recent optic nerve crush studies have demonstrated substantial axon regeneration and proper distal targeting (reviewed in Laha et al., 2017). However, the potential for the adult mammalian CNS to reestablish synaptic specificity following injury or disease remained unknown. In this study, we showed that the precise connectivity between specific cell types established during development can be reestablished in the adult mammalian CNS after injury. However, circuit reassembly does not entirely mimic circuit assembly during development.

Selective synaptic connections between specific neuronal cell types are known to form during development. Beier et al. showed that new synaptic connections can be established in the adult mammalian retina (rabbit) after injury, but the synaptic precision within the new neural circuits remained unknown [20]. Circuit reassembly with synaptic precision is known to occur in adult non-mammalian species, albeit with reduced selectivity [24,25]. We aimed to determine if synaptic precision could be recreated in the adult mammalian CNS.

Circuit repair can be split into at least two descriptive phases: partner discovery and synaptic reassembly. During partner discovery, S-cone bipolar cell dendritic exploration ends at S-cone axon terminals, which are their preferred presynaptic partners. Since we cannot distinguish between (a) S-cone synapses that diverge to an edge S-cone bipolar cell and a normal S-cone bipolar cell from (b) S-cone synapses that diverge to two normal S-cone bipolar cells (Figure 3D), we infer that a new synapse is assembled without displacing the already existing synapse to a healthy S-cone bipolar cell. Furthermore, during the partner discovery process, the restructured dendrites pass by numerous M-cone axon terminals without forming apparent synapses. Together, these findings indicate that an ability to form selective synapses to S-cones is present in the adult S-cone bipolar cells. It is important to note that while the confluence of the obtained evidence leaves little doubt that new synapses are formed, electron microscopy would be required to further characterize the synaptic nano-structure. Additionally, electrical recordings of the light responses of the restructured S-cone bipolar cells would be required to measure the functional properties of the newly-formed synapses. The scarcity of the reassembled synapses and the absence of selective S-cone bipolar cell labeling in live tissue make both electron microscopy and electrophysiology studies difficult. In the future, large-scale calcium imaging of bipolar cell activity in response to S-cone isolating stimulus might help to reveal functional details of the new synapses.

The findings in this study are encouraging to the restoration of sight following photoreceptor degeneration in diseases like age-related macular degeneration (AMD) and retinitis pigmentosa. Photoreceptor replacement has been proposed as a therapy for vision loss caused by such diseases [26]. Photoreceptor replacement strategies rely on the inherent ability of the deafferented retina to reconnect properly with the new photoreceptors. We have shown that synaptic selectivity required for a chromatic pathway can be reestablished during circuit repair in the adult mammalian retina.

We do not expect circuit repair mechanisms to be perfectly conserved across species. When discussing the potential therapeutic implications of our findings, it is important to consider how the ground squirrel retina resembles and differs from primate retinas. Both the central primate retina (including human) and ground squirrel retinas are cone-rich. Importantly, the ground squirrel S-cone bipolar cell is a unique analogue of the midget bipolar cells of the central primate retina, as both receive direct input from a single cone. This connectivity in the central primate retina is necessary for high spatial acuity vision, which is lost in the course of AMD. We show that after losing their single photoreceptor inputs, S-cone bipolar cells can synapse with a single cone photoreceptor again. This finding suggests that midget bipolar cells in the central primate retina might be able to form new synapses with single,

newly introduced, photoreceptors. Such preservation of the photoreceptor to bipolar cell convergence is necessary to restore high visual acuity.

Ground squirrels are unique from many mammals in that they are hibernating animals. Hibernation in ground squirrels has been shown to result in significant changes at the pre-synaptic side of cone photoreceptor to cone bipolar cell synapses. During hibernation the cone photoreceptor ribbon synapse will undergo partial disassembly, followed by reassembly upon awakening from hibernation [27–30]. The post-synaptic side of the cone synapse does not seem to exhibit similar changes [28]. It is possible that cone photoreceptors in the ground squirrel retina have access to unique mechanisms that facilitate synaptic reassembly during circuit repair that are not available in the primate retina.

Compared to circuit repair, circuit formation in the CNS is relatively well studied. Are the cellular and molecular mechanisms involved in circuit formation during development the same as the mechanisms in use during the adult circuit reassembly? Although molecular mechanisms are beyond this study, we can make a few observations regarding cellular mechanisms involved in the adult circuit reassembly. We show that deafferented S-cone bipolar cells effectively expand their dendritic field by creating new dendritic branches, which elongate and explore within the OPL until encountering an S-cone and creating a new synapse. Likewise, strategies for dendritic expansion during normal development are known to include the creation of new dendritic branches, as well as dendritic elongation [4,31,32]. However, developmental dendritic expansion strategies are known to differ even amongst bipolar cell types [33]. Thus, it is possible that the S-cone bipolar cells in the adult ground squirrel retina have retained developmental mechanisms that were previously acting during development.

Dendritic pruning is a common cellular mechanism employed during circuit refinement in the developmental period and it is markedly missing over the course of our study in the adult ground squirrel retina. The lack of dendritic pruning might be caused by (a) our study being too short to observe it, (b) the absence of dendritic pruning of S-cone bipolar cells in the adult retina, or (c) S-cone bipolar cells lacking the ability to prune their dendrites in both the developing and adult retinas. Since the timeline for normal S-cone bipolar cell development and the strategies they use to find S-cones is unknown, we cannot conclusively say if the lack of dendritic pruning we observed is due to missing refinement mechanisms in the adult retina. However, since the dendritic trees of the deafferented S-cone bipolar cells involved in circuit reassembly do not entirely resemble that of normal adult S-cone bipolar cells, it is important to note that circuit repair in the adult retina can recreate only some aspects of a normal stereotypic circuit.

Our findings indicate that while some aspects of circuit reassembly in the adult mammalian retina resemble developmental mechanisms (e.g. dendritic expansion and synaptic precision), other developmental mechanisms may be missing (e.g. dendrite refinement).

STAR METHODS

CONTACT FOR REAGENT AND RESOURCE SHARING

Further information and requests for resources should be directed to and will be fulfilled by the corresponding author, Alexander Sher (sashake3@ucsc.edu).

EXPERIMENTAL MODEL AND SUBJECT DETAILS

13-Lined Ground Squirrels—Adult thirteen-lined ground squirrels were used in accordance with the Association for Research in Vision and Ophthalmology Statement Regarding the Use of Animals in Ophthalmic and Vision Research. A total of 10 adult (postnatal day 80 and older) squirrels, of either sex, were used for this research. Squirrels were purchased from the University of Wisconsin Oshkosh Squirrel Colony [34].

METHOD DETAILS

Selective Photocoagulation—Squirrels were first anesthetized briefly with isoflurane and then injected intramuscularly with a solution of ketamine hydrochloride xylazine diluted with sterile water. Once the squirrels were anesthetized, typically within 15 minutes post-injection, a single drop of both 1% tropicamide and 2.5% phenylephrine hydrochloride was applied to each eye to dilate the pupil. Lesions were applied to both the superior and inferior retina with a scanning laser (PASCAL, 532nm) using a custom scanning software. A laser beam of 100μm in diameter was scanned once over 1.0mm length of the retina at 1.0m/s scanning velocity and power of 2.0W. Laser settings were titrated in preliminary experiments that checked for selective photoreceptor destruction with immunohistochemistry. Line lesions showed an immediate whitening of the fundus when placed *in vivo* in squirrel retinas. Lesions of 200μ m in width were created by overlapping three 100μm-wide scans, such that the overlap was equal to half the beam diameter.

Immunohistochemistry—To investigate retinal response to the photoreceptor loss, animals were euthanized at various time points after the ablation procedure. After enucleation, pieces of retinal tissue were separated from the choroid and sclera, and placed in 4% paraformaldehyde, pH 7.4, for 12 minutes at room temperature. Retina was washed 6 times for 30 minutes in a modified PBS (mPBS) solution (0.1M, pH 7.4, 0.1% NaN3, 0.5% Triton X-100) at room temperature, blocked for 2 days in mPBS with 3% donkey serum at 4°C and incubated in primary and then secondary antibodies for 5 and 2 days, respectively, in 1% donkey serum in mPBS at 4°C. Retinas were washed 6 times for 30 minutes in mPBS before being mounted onto slides, with 4,6-diamidinno-2-phenylindole (DAPI) (0.2μg/mL Sigma-Aldrich) added during the second-to-last wash. We used the following primary antibodies: rabbit anti-hyperpolarization-activated cyclic nucleotide-gated channel 4 (HCN4; 1:400, Alomone Labs, APC-052), goat anti-S-opsin (1:100, Santa Cruz Biotechnology, sc-14363), goat anti-ionotropic glutamate receptor 5 (iGluR5; 1:50, Santa Cruz Biotechnology, sc-7616), mouse anti-C-terminal binding protein 2 (CtBP2; 1:400, BD Biosciences, 612044), goat anti-CtBP2 (1:100, Santa Cruz Biotechnology, sc-5966), goat anti-metabotropic glutamate receptor 6 (mGluR6; 1:1000, a gift from Stephen Massey) [35]. Occasionally, to improve our ability to locate S-cone axon terminals, goat anti-S-opsin and goat anti-iGluR5 were paired together in the same primary incubation period. The following

secondary antibodies were paired with the appropriate primary antibodies (all used at 1:1000, Life Technologies, Alexa Fluor variety, catalog numbers printed respectively in list): donkey anti-goat 555nm or 647nm (A-21432 or A-21447), donkey anti-mouse 488nm, 555nm or 647nm (A-21202, A-31570, or A-31571), and donkey anti-rabbit 488nm, 555nm or 647nm (A-21206, A-31572, or A-31573). Retinas were mounted with Vectashield (H-1000; Vector Laboratories) on a glass slide, photoreceptor-side down, with small pieces of molding clay between the slide and the coverslip. The molding clay was carefully depressed until the coverslip rested against the retina.

Image Acquisition and Image Analysis—Retinas were imaged on a Leica SP5 confocal microscope with an oil immersion lens (63x NA 1.4). Voxel size was set by 532nm Nyquist values and each optical plane was imaged 3–4 times. Fiji software (NIH) was used to generate Z-projections and cross sections from Z-stacks [36]. Fiji plugins Pairwise Stitching and Grid/Collection Stitching were both used to stitch tiled images [37].

HCN4-stained bipolar cell dendritic trees were traced using the Fiji Simple Neurite Tracer plugin [38]. The tracing was done on confocal Z-stacks of HCN4 stains. An S-cone bipolar cell soma was identified in the stack and the beginning of the primary dendrite was manually marked at the edge of the soma. The dendrite was traced out to the OPL using the semi-automated tracing software Simple Neurite Tracer, which attempts to connect two user-defined inputs along the dendrite. Tracing was completed on stacks without additional channels to show S-cone locations (only the HCN4 channel was used for tracing). Completed traces were imported to custom MATLAB (Mathworks) scripts. S-cone axon terminal locations, identified by a lack of iGluR5 staining [7] and lesion edge traces, were marked as regions of interest (ROIs) in Fiji and then imported to MATLAB. The OPL ROI was constructed by creating a binary image of an iGluR5 or CtBP2 stain and dilating and then closing the image in 3D [39]. The OPL was defined by the binary image after an additional dilation step that used a horizontal line to close the ablation zone. In MATLAB, dendritic trees of HCN4-stained bipolar cells were defined as the traces that overlapped with the OPL. We defined S-cone bipolar cells as edge cells if their dendritic trees crossed the ablation zone edge. Dendritic tree fields were defined as convex polygons that outlined the dendritic tree of traced cells. The dendritic field area was the area of this polygon. The dendritic projection vector of a single cell was calculated as a vector sum of the projection vectors of individual dendrites (see Figure 2D for an example). The angles of the vectors were defined relative to the lesion orientation: vertical direction was parallel and horizontal was perpendicular to the lesion's edge. The directionality index (DI) is defined as the number of dendrites, per cell, projecting away from lesion center minus the number of dendrites projecting towards the lesion center over the total number of dendrites. Therefore, if a cell preferred to orient all of its dendrites out of the photoreceptor ablation zone, it would have a DI = 1, DI = 0 would indicate no direction preference, and DI = −1, would correspond to dendrites projecting further into the ablation zone. Cells with only a single dendritic stalk were excluded from the projection vector and DI analyses.

To quantify the overlap between mGluR6 staining and HCN4 dendritic traces, the individual channels were converted to binary images with the automated mask thresholding feature in Fiji, using the "Moments" method for each stack [40]. The "Moments" thresholding method

was applied across the entire Z-stack of the image of a single lesion, as opposed to being calculated for each slice, and resulted in a 3D mask that was imported to MATLAB. For the HCN4 binary mask, all staining that did not coincide with the previously mapped dendritic traces was removed. For the mGluR6 channel, all staining that did not coincide with the HCN4 binary mask was removed. Glutamate receptor volume was calculated at the locations of previously mapped S-cone axon terminals. Glutamate receptor volume was then normalized to the average of glutamate receptor volume at all S-cones. In the event that we identified a cluster that did not coincide with the mapped S-cone axon terminals, we labeled this an M-cone synapse.

QUANTIFICATION AND STATISTICAL ANALYSIS—Statistical criteria used are indicated in the main text and are two-tailed unless indicated otherwise.

ACKNOWLEDGEMENTS

This work was supported by Burroughs Wellcome Fund Career Award at the Scientific Interface, Pew Charitable Trusts Scholarship in the Biomedical Sciences, National Institutes of Health Grant EY023020-01 to A.S., and Fight for Sight Summer Fellowship to C.B. We thank Stephen Massey for providing the mGluR6 antibody; Ben Abrams for microscopy assistance and maintaining microscopy centers; David Feldheim, and Jena Yamada for helpful discussions throughout the project.

REFERENCES

1. Sanes JR, and Yamagata M (2009). Many Paths to Synaptic Specificity. Annu. Rev. Cell Dev. Biol 25, 161–195. [PubMed: 19575668]
2. Margeta MA, and Shen K (2010). Cellular and Molecular Mechanisms of Synaptic Specificity. Mol. Cell. Neurosci 43, 261–267. [PubMed: 19969086]
3. de Wit J, and Ghosh A (2015). Specification of synaptic connectivity by cell surface interactions. Nat. Rev. Neurosci 17, 4–4. [PubMed: 26656256]
4. Luo J, McQueen PG, Shi B, Lee C-H, and Ting C-Y (2016). Wiring dendrites in layers and columns. J. Neurogenet 30, 69–79. [PubMed: 27315108]
5. Zhang C, Kolodkin AL, Wong RO, and James RE (2017). Establishing Wiring Specificity in Visual System Circuits: From the Retina to the Brain. Annu. Rev. Neurosci 40, annurev-neuro-072116-031607.
6. Riccomagno MM, and Kolodkin AL (2015). Sculpting Neural Circuits by Axon and Dendrite Pruning. Annu. Rev. Cell Dev. Biol 31, 779–805. [PubMed: 26436703]
7. Li W, and DeVries SH (2004). Separate blue and green cone networks in the mammalian retina. Nat. Neurosci 7, 751–6. [PubMed: 15208635]
8. Li W, and DeVries SH (2006). Bipolar cell pathways for color and luminance vision in a dichromatic mammalian retina. Nat. Neurosci 9, 669–75. [PubMed: 16617341]
9. Sher A, and Devries SH (2012). A non-canonical pathway for mammalian blue-green color vision. Nat. Neurosci 15, 952–3. [PubMed: 22634728]
10. Field GD, Sher A, Gauthier JL, Greschner M, Shlens J, Litke AM, and Chichilnisky EJ (2007). Spatial properties and functional organization of small bistratified ganglion cells in primate retina. J. Neurosci 27, 13261–72. [PubMed: 18045920]
11. Field GD, Gauthier JL, Sher A, Greschner M, Machado T, Jepson LH, Shlens J, Gunning DE, Mathieson K, Dabrowski W, et al. (2010). Functional connectivity in the retina at the resolution of photoreceptors. Nature 467, 673–7. [PubMed: 20930838]
12. Dacey DM, and Packer OS (2003). Colour coding in the primate retina: diverse cell types and cone-specific circuitry. Curr. Opin. Neurobiol 13, 421–427. [PubMed: 12965288]

13. Crook JD, Davenport CM, Peterson BB, Packer OS, Detwiler PB, and Dacey DM (2009). Parallel ON and OFF cone bipolar inputs establish spatially coextensive receptive field structure of blue-yellow ganglion cells in primate retina. J. Neurosci 29, 8372–87. [PubMed: 19571128]
14. Dacey DM, and Lee BB (1994). The “blue-on” opponent pathway in primate retina originates from a distinct bistratified ganglion cell type. Nature 367, 731–5. [PubMed: 8107868]
15. Calkins DJ, Tsukamoto Y, and Sterling P (1998). Microcircuitry and mosaic of a blue-yellow ganglion cell in the primate retina. J. Neurosci 18, 3373–85. [PubMed: 9547245]
16. Marshak DW, and Mills SL (2014). Short-wavelength cone-opponent retinal ganglion cells in mammals. Vis. Neurosci 31, 165–75. [PubMed: 24759445]
17. Haverkamp S (2005). The Primordial, Blue-Cone Color System of the Mouse Retina. J. Neurosci 25, 5438–5445. [PubMed: 15930394]
18. Herr S, Klug K, Sterling P, and Schein S (2003). Inner S-Cone Bipolar Cells Provide All of the Central Elements for S Cones in Macaque Retina 201, 185–201.
19. Puller C, Ondreka K, and Haverkamp S (2011). Bipolar cells of the ground squirrel retina. J. Comp. Neurol 519, 759–74. [PubMed: 21246553]
20. Beier C, Hovhannisyan A, Weiser S, Kung J, Lee S, Yeong Lee D, Huie P, Dalal R, Palanker D, and Sher A (2017). Deafferented adult rod bipolar cells create new synapses with photoreceptors to restore vision. J. Neurosci 37, 2570–16.
21. Dunn F. a. (2015). Photoreceptor Ablation Initiates the Immediate Loss of Glutamate Receptors in Postsynaptic Bipolar Cells in Retina. J. Neurosci 35, 2423–2431. [PubMed: 25673837]
22. Kryger Z, Galli-Resta L, Jacobs GH, and Reese BE (1998). The topography of rod and cone photoreceptors in the retina of the ground squirrel. Vis. Neurosci 15, 685–691. [PubMed: 9682870]
23. Laha B, Stafford BK, and Huberman AD (2017). Regenerating optic pathways from the eye to the brain. Science 356, 1031–1034. [PubMed: 28596336]
24. Yoshimatsu T, D’Orazi FD, Gamlin CR, Suzuki SC, Suli A, Kimelman D, Raible DW, and Wong RO (2016). Presynaptic partner selection during retinal circuit reassembly varies with timing of neuronal regeneration in vivo. Nat. Commun 7, 10590. [PubMed: 26838932]
25. D’Orazi FD, Zhao X-F, Wong RO, and Yoshimatsu T (2016). Mismatch of Synaptic Patterns between Neurons Produced in Regeneration and during Development of the Vertebrate Retina. Curr. Biol, 1–12.
26. Jayakody SA, Gonzalez-Cordero A, Ali RR, and Pearson RA (2015). Cellular strategies for retinal repair by photoreceptor replacement. Prog. Retin. Eye Res 46, 31–66. [PubMed: 25660226]
27. Kuwabara T (1975). Cytologic changes of the retina and pigment epithelium during hibernation. Invest. Ophthalmol 14, 457–467. [PubMed: 166050]
28. Mehta B, Snellman J, Chen S, Li W, and Zenisek D (2013). Synaptic Ribbons Influence the Size and Frequency of Miniature-like Evoked Postsynaptic Currents. Neuron 77, 516–527. [PubMed: 23395377]
29. Merriman DK, Sajdak BS, Li W, and Jones BW (2016). Seasonal and post-trauma remodeling in cone-dominant ground squirrel retina. Exp. Eye Res 150, 90–105. [PubMed: 26808487]
30. Qiao F, Chen S, Merriman D, and Li W (2013). Mechanisms of Photoreceptor Synaptic Ribbon Plasticity in the Hibernating Ground Squirrel Retina
31. D’Orazi FD, Suzuki SC, and Wong RO (2014). Neuronal remodeling in retinal circuit assembly, disassembly, and reassembly. Trends Neurosci 37, 594–603. [PubMed: 25156327]
32. Lefebvre JL, Sanes JR, and Kay JN (2015). Development of Dendritic Form and Function. Annu. Rev. Cell Dev. Biol 31, 741–777. [PubMed: 26422333]
33. Dunn FA, and Wong ROL (2012). Diverse Strategies Engaged in Establishing Stereotypic Wiring Patterns among Neurons Sharing a Common Input at the Visual System ‘ s First Synapse. J. Neurosci 32, 10306–10317. [PubMed: 22836264]
34. Merriman DK, Lahvis G, Jooss M, Gesicki JA, and Schill K (2012). Current practices in a captive breeding colony of 13-lined ground squirrels (Ictidomys tridecemlineatus). Lab Anim. (NY) 41.
35. Pan F, and Massey SC (2007). Rod and Cone Input to Horizontal Cells in the Rabbit Retina. J. Comp. Neurol 500, 815–831. [PubMed: 17177254]

36. Schindelin J, Arganda-Carreras I, Frise E, Kaynig V, Longair M, Pietzsch T, Preibisch S, Rueden C, Saalfeld S, Schmid B, et al. (2012). Fiji: an open-source platform for biological-image analysis. Nat. Methods 9, 676–82. [PubMed: 22743772]

37. Preibisch S, Saalfeld S, and Tomancak P (2009). Globally optimal stitching of tiled 3D microscopic image acquisitions. Bioinformatics 25, 1463–1465. [PubMed: 19346324]

38. Longair MH, Baker DA, and Armstrong JD (2011). Simple neurite tracer: Open source software for reconstruction, visualization and analysis of neuronal processes. Bioinformatics 27, 2453–2454. [PubMed: 21727141]

39. Legland D, Arganda-Carreras I, and Andrey P (2016). MorphoLibJ: integrated library and plugins for mathematical morphology with ImageJ. Bioinformatics 32, btw413.

40. Tsai W-H (1985). Moment-preserving thresolding: A new approach. Comput. Vision, Graph. Image Process 29, 377–393.

Highlights

- Circuit repair in the adult mammalian retina recreates stereotypic selective wiring
- Adult S-cone bipolar cells establish selective synapses with S-cones after injury
- Circuit reassembly strategies in the adult CNS resemble developmental strategies

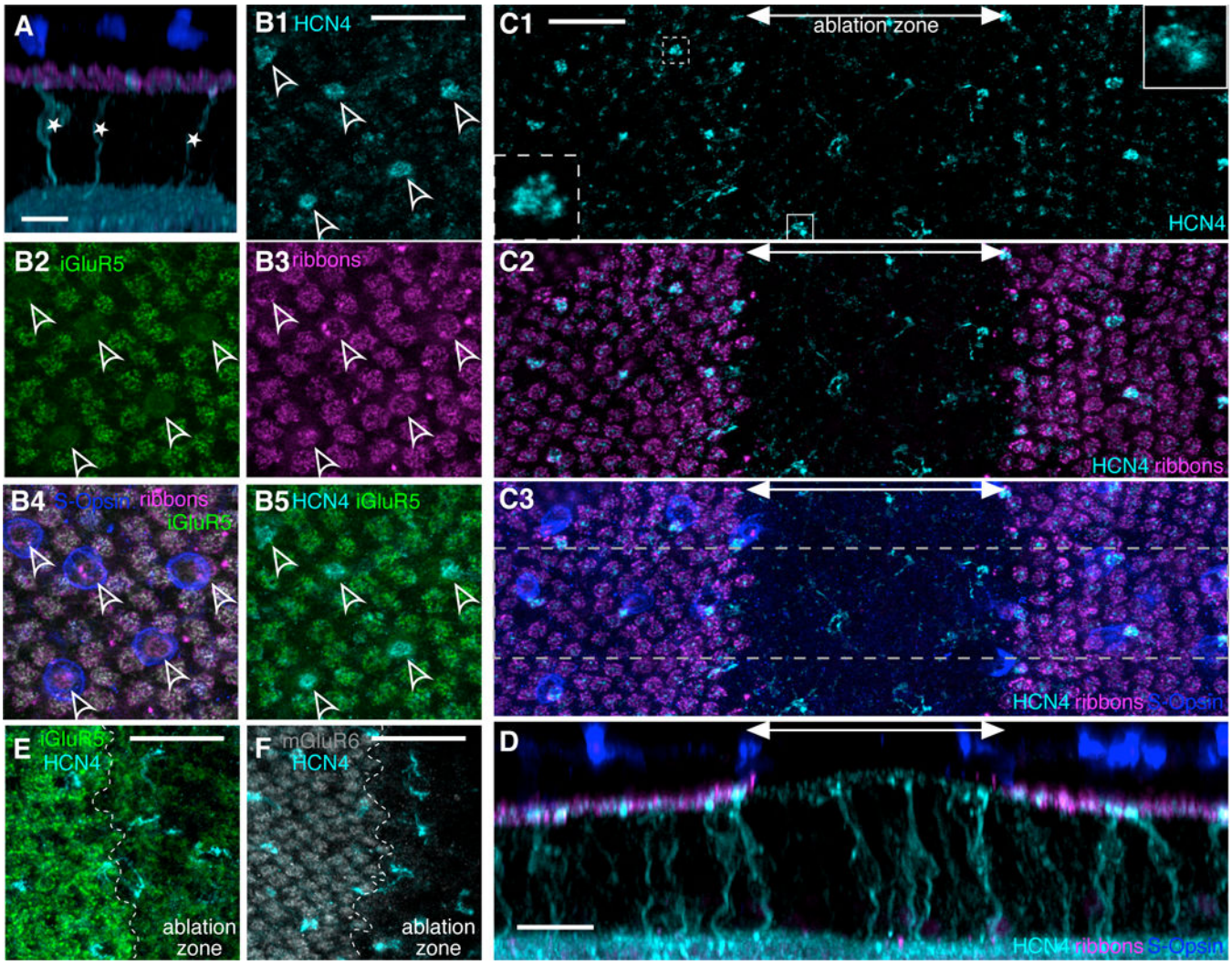

Figure 1. S-cone bipolar cells are completely deafferented by local photoreceptor ablation.

A. Confocal reconstruction of the healthy retina cross section. S-cone bipolar cells are immunostained for HCN4 (cyan). S-cone bipolar cell bodies (*) sit in the inner nuclear layer and send a single dendrite towards the photoreceptor ribbons (CtBP2, magenta) in the outer plexiform layer (OPL) to synapse with a single S-cone photoreceptor (outer segments stained with S-opsin, blue). **B1**. Maximal Z-projection in the OPL of healthy retina. Bright HCN4 puncta define locations of the S-cone bipolar cells' dendritic tips (arrowheads). **B2**. In the same field of view as in (**B1**), iGluR5 immunostaining marks the location of M-cone axon terminal synapses, but not S-cone axon terminals. **B3**. Photoreceptor ribbons (CtBP2) mark both M- and S-cone axon terminal locations. **B4**. S-opsin staining from the outer nuclear layer (ONL) is overlaid with projections from the OPL, (**B2**) and (**B3**). S-cone cell bodies, though slightly offset from their axon terminals, align with the marked S-cone axon terminal locations. **B5**. Overlay of (**B1**) and (**B2**). S-cone bipolar cell dendritic tips (HCN4) terminate at S-cone axon terminals (lack of iGluR5). **C1.** Maximal Z-projection of the OPL of a 1-week-old ablation zone. S-cone bipolar cell dendritic tips (HCN4, cyan) are visible inside and outside the ablation zone. A double headed arrow marks the approximate width of

the ablation zone area. Insets: Dendritic tip of an S-cone bipolar cell outside (dashed outline) and inside (solid outline) ablation zone. Inset images show a 5×5μm area of a single 0.3μm thick optical plane. **C2**. The ablation zone (marked by double headed arrow) is identified by the lack of photoreceptor ribbons (CtBP2, magenta). **C3**. S-opsin immunostaining from the ONL overlaid with (**C2**) marks S-cone locations. S-opsin staining is absent in the 1-week-old ablation zone. **D.** Cross section of the retinal region outlined in gray dashed lines in (**C3**). S-cone bipolar cell dendritic stalks extend vertically towards the OPL inside and outside the ablation zone. **E** and **F** show a portion of the OPL at the edge of a 1-week-old ablation zone. The ablation zone is to the right of the ablation zone edge (edge marked by dashed white line). Both iGluR5 (**E**) and mGluR6 (**F**) labeling is decreased inside the lesion. Scale bars are 20μm in all panels.

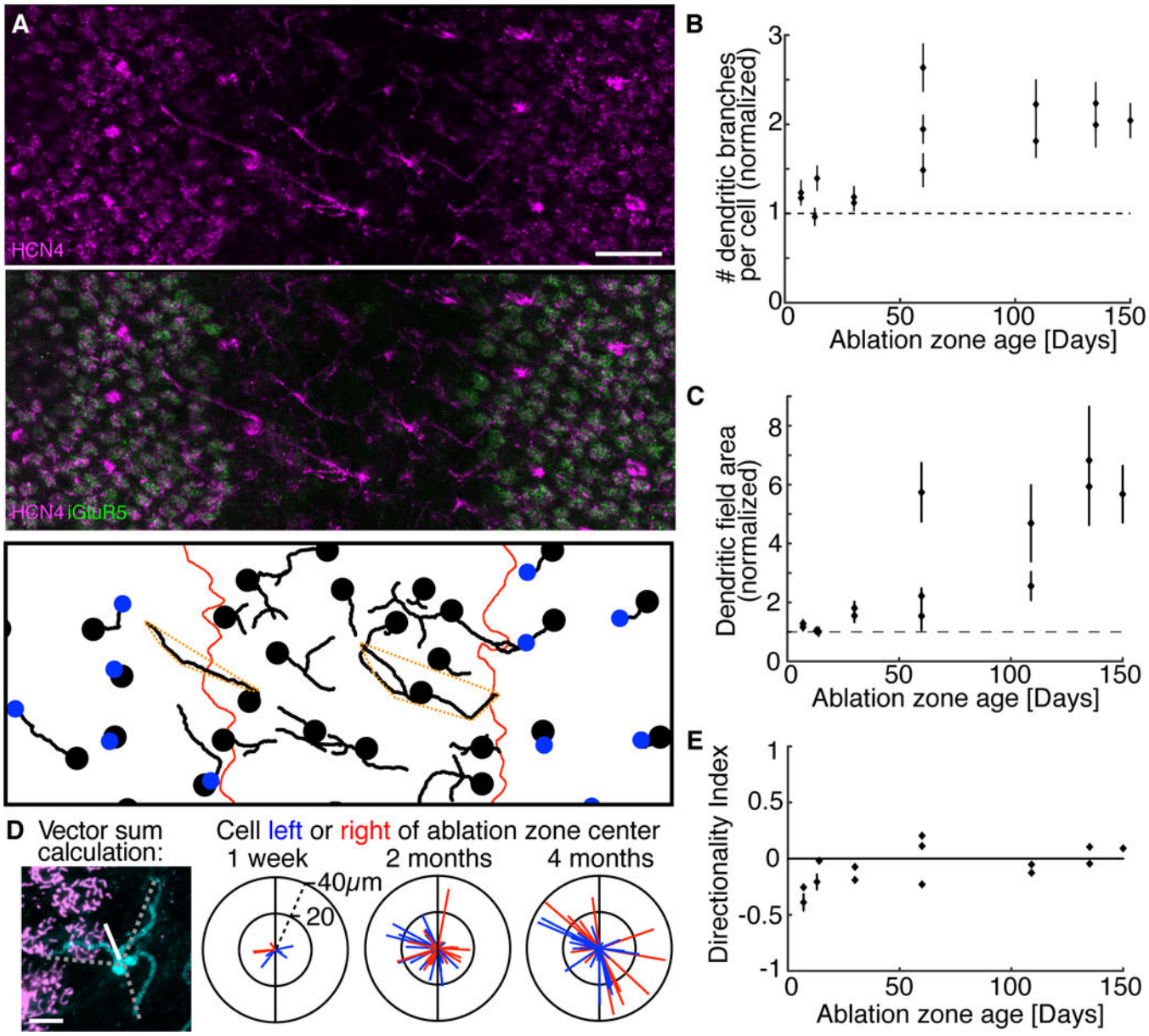

Figure 2. S-cone bipolar cells expand their dendritic trees in response to deafferentation.

A. Numerous dendritic branches of S-cone bipolar cells (HCN4, cyan) visible in a 60- day-old ablation zone (area lacking iGluR5, green). Bottom panel: S-cone bipolar cell dendrites (traced in 3D). Bipolar cell soma locations and S-cone axon terminals are marked by the black dots and blue dots, respectively. Red lines mark ablation zone border. Dashed orange polygons outline the dendritic fields of example cells. Scale bar 20μm. **B.** The average number of dendritic branches per cell inside the ablation zone normalized to the average dendritic branch number per cell outside the ablation zone (data from 14 ablation zones are shown as mean ± SEM, n ≥ 30 cells for each data point). S-cone bipolar cells inside the ablation zone have more dendritic branches than S-cone bipolar cells outside the ablation zone (binomial probability, $p < 1e\text{-}6$ for all ablation zones 60 days and older). Dendritic branches per cell increase with lesion age (correlation coefficient = 0.74, $p < 2e\text{-}3$). **C.**

Dendritic field area (see dashed orange polygons in **A** for examples) dependence on ablation zone age for the same 14 ablation zones as in B. Dendritic field areas of cells inside each ablation zone are normalized by dendritic field areas in the surrounding retina. Dendritic fields inside ablation zones are larger than dendritic fields outside of the ablation zone (KS test, $p < 0.001$ for all lesions 60 days and older, $n \geq 30$ cells for each ablation zone). Dendritic field areas increase with lesion age (correlation coefficient = 0.85, $p < 2e\text{-}4$). **D.** Left panel: Dendritic branch reach and angle (dashed lines) of an S-cone bipolar cells (cyan) were summed as vectors to estimate the dendritic directionality of the cell (white line). Three right panels: Vectors representing individual cells were colored red/blue if the cell was to the right/left of the ablation zone center, respectively. The ablation zone has been oriented vertically (black line) in each plot. Scale bar 5μm. **E.** Average directionality index of S-cone bipolar cells calculated in the 14 ablation zones at different times after photoreceptor ablation (mean ± SEM, $n \geq 10$ cells for each ablation zone). Deafferented cell dendrites do not show consistent directional bias.

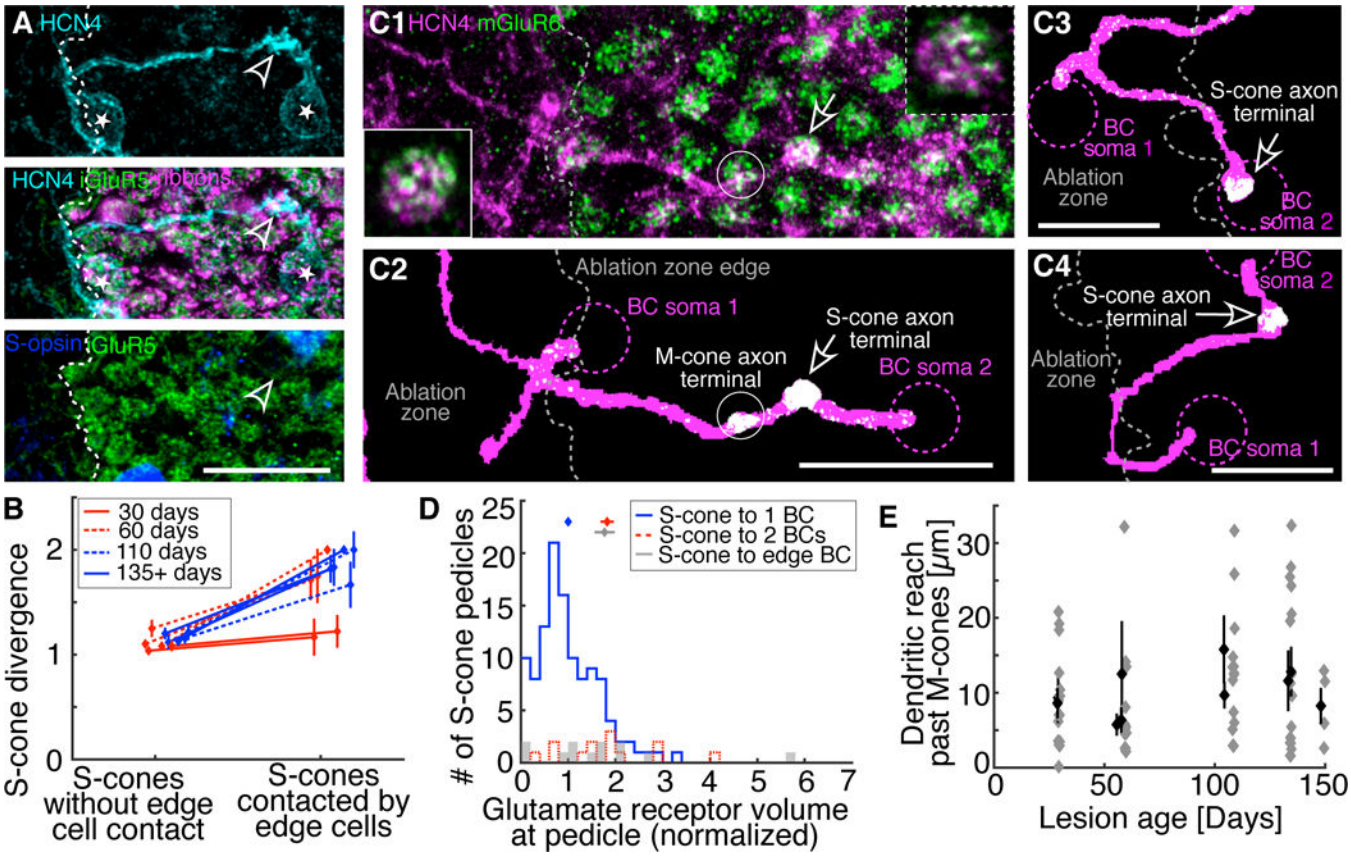

Figure 3. Deafferented S-cone bipolar cell dendrites bypass M-cones to synapse with new S-cones.

A. Two S-cone bipolar cells (somas marked by *) contact the same S-cone axon terminal (arrowhead). The dendritic tree of the leftmost bipolar cell begins within the ablation zone (area lacking iGluR5, green and CtBP2, magenta). The S-cone bipolar cell dendrite travels parallel to the OPL, through M-cone territory (iGluR5, green), to contact the S-cone. Scale bar 20μm. **B.** S-cones contacted by edge cells are significantly more likely to diverge to more than 1 S-cone bipolar cell than S-cones that are not contacted by edge cells (binomial probability, $p \leq 1e\text{-}7$ for ablation zones 60 days and older, $n \geq 14$ cells with and without contact in each age group: 30 days, 60 days, 110 days and 135–150 days). **C1.** S-cone bipolar cell dendrites (HCN4, magenta) and mGluR6 (green) located at cone axon terminals visible in a maximal Z-projection of the OPL. Insets: HCN4 and mGluR6 overlap in a single 0.3μm thick optical plane at S-cone bipolar cell dendritic tips. Inset with solid outline: S-cone terminal contacted by a restructured S-cone bipolar cell (same synapse as indicated by arrow). Inset with dashed outline: S-cone terminal contacted by a non-restructured S-cone bipolar cell, far from the ablation zone edge not shown in the image. Insets are 5×5μm. **C2:** Z-projection of **C1** after conversion into binary images. mGluR6 staining not overlapping with HCN4 dendritic traces was removed, leaving only colocalized mGluR6 (white). See Methods for details. Additional examples in **C3** and **C4**. In all **C** panels, two S-cone bipolar cells (dashed magenta circles indicate somas) synapse with a single S-cone (arrow). In each case, one S-cone bipolar cell's dendritic tree begins within the ablation zone and travels out to make the synapse, where mGluR6 is present. We rarely (n = 4/23 edge cells) found

evidence for an M-cone synapse. See **C2** for the rare example. Scale bars 20μm. **D.** The volume overlap between HCN4 and mGluR6 at S-cone axon terminals (mean ± SEM above histograms). mGluR6 volume at individual S-cone terminals is normalized to the average mGluR6 volume at all S-cone terminals. S-cones connected to 1 S-cone bipolar cell have less mGluR6 volume than S-cones diverging to 2 S-cone bipolar cells (Student's t-test, p = 8e-5), including S-cones that diverge to edge cells (p = 0.0011). S-cones in healthy retina diverging to 2 S-cone bipolar cells have the same mGluR6 volume as S-cones that diverge to edge cells (p = 0.92). **E.** The dendritic reach through M-cone territory of individual edge bipolar cells that contact an S-cone (grey diamonds). Black diamonds show mean ± SEM of the 10 ablation zones that are 30 days and older.

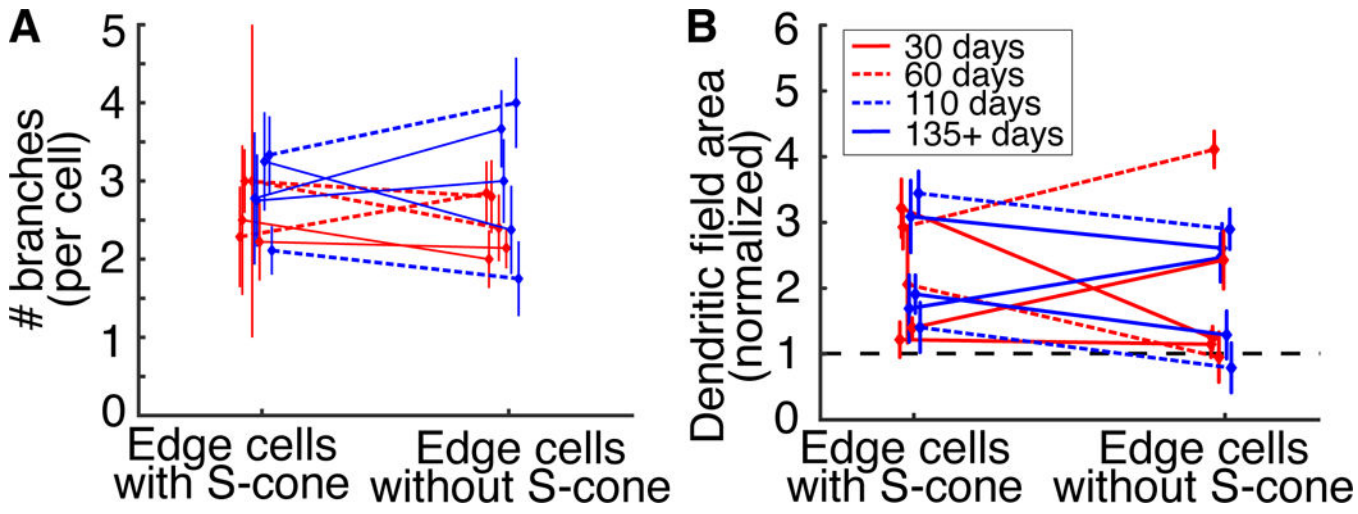

Figure 4. Dendritic tree simplification does not occur after new S-cone synapses are established.

A. The number of dendritic branches per edge cell with or without S-cones. Mean ± SEM. S-cone contact does not affect the number of dendritic branches per cell (binomial probability, $p > 0.06$, $n \geq 8$ cells with and without S-cones in each age group). **B.** The dendritic field area of edge cells with and without S-cones. The dendritic fields of edge cells have been normalized to the dendritic fields of cells within the ablation zone. Mean ± SEM. Dendritic field areas do not change with S-cone contact (KS test, $p > 0.8$, $n \geq 8$ cells with and without S-cones in each age group).

KEY RESOURCES TABLE

REAGENT or RESOURCE	SOURCE	IDENTIFIER
Antibodies		
Rabbit polyclonal anti-HCN4	Alomone Labs	APC-052; RRID: AB_2039906
Goat polyclonal anti-S-opsin	Santa Cruz Biotechnology	sc-14363; RRID: AB_2158332
Goat polyclonal anti-iGluR5	Santa Cruz Biotechnology	sc-7616; RRID: AB_641048
Mouse monoclonal anti-CtBP2	BD Biosciences	612044; RRID: AB_399431
Goat polyclonal anti-CtBP2	Santa Cruz Biotechnology	sc-5966; RRID: AB_2086774
Goat polyclonal anti-mGluR6	[19]	N/A
Experimental Models: Organisms/Strains		
13-lined Ground Squirrel	[20]	N/A
Software and Algorithms		
Fiji (Fiji is Just Image J)	[21]	N/A
Fiji Simple Neurite Tracer plugin	[23]	N/A
MATLAB	Mathworks	R2017b